HHS Public Access

Author manuscript

Magn Reson Med. Author manuscript; available in PMC 2020 June 02.

Published in final edited form as:

Magn Reson Med. 2016 March ; 75(3): 1018–1029. doi:10.1002/mrm.25636.

4D Spiral Imaging of Flows in Stenotic Phantoms and Subjects with Aortic Stenosis

MJ Negahdar[1,2], **Mo Kadbi**[4], **Michael Kendrick**[2], **Marcus F. Stoddard**[2,3], **Amir A. Amini**[1,2,*]

[1]Medical Imaging Lab, Department of Electrical and Computer Engineering, University of Louisville, Louisville, Kentucky, USA

[2]Robley Rex Veterans Affairs Medical Center, Louisville, Kentucky, USA

[3]Division of Cardiovascular Medicine, University of Louisville, School of Medicine, Louisville, Kentucky, USA

[4]Philips Medical Systems, Philips Healthcare, Cleveland, Ohio, USA

Abstract

Purpose: The utility of four-dimensional (4D) spiral flow in imaging of stenotic flows in both phantoms and human subjects with aortic stenosis is investigated.

Methods: The method performs 4D flow acquisitions through a stack of interleaved spiral k-space readouts. Relative to conventional 4D flow, which performs Cartesian readout, the method has reduced echo time. Thus, reduced flow artifacts are observed when imaging high-speed stenotic flows. Four-dimensional spiral flow also provides significant savings in scan times relative to conventional 4D flow.

Results: In vitro experiments were performed under both steady and pulsatile flows in a phantom model of severe stenosis (one inch diameter at the inlet, with 87% area reduction at the throat of the stenosis) while imaging a 6-cm axial extent of the phantom, which included the Gaussian-shaped stenotic narrowing. In all cases, gradient strength and slew rate for standard clinical acquisitions, and identical field of view and resolution were used. For low steady flow rates, quantitative and qualitative results showed a similar level of accuracy between 4D spiral flow (echo time [TE] = 2 ms, scan time = 40 s) and conventional 4D flow (TE = 3.6 ms, scan time = 1:01 min). However, in the case of high steady flow rates, 4D spiral flow (TE = 1.57 ms, scan time = 38 s) showed better visualization and accuracy as compared to conventional 4D flow (TE = 3.2 ms, scan time = 51 s). At low pulsatile flow rates, a good agreement was observed between 4D spiral flow (TE = 2 ms, scan time = 10:26 min) and conventional 4D flow (TE = 3.6 ms, scan time = 14:20 min). However, in the case of high flow-rate pulsatile flows, 4D spiral flow (TE = 1.57 ms, scan time = 10:26 min) demonstrated better visualization as compared to conventional 4D flow (TE = 3.2 ms, scan time = 14:20 min). The feasibility of 4D spiral flow was also investigated in five normal volunteers and four subjects with mild-to-moderate aortic stenosis. The approach

*Correspondence to: Amir A. Amini, 409 Lutz Hall, University of Louisville, Louisville, KY, 40292. amir.amini@louisville.edu.

Correction added after online publication 6 May 2015. Due to a publisher's error, grammatical corrections made during the proof stage by the authors in the Introduction and Methods sections were not implemented before online publication, and have been updated in this version.

achieved TE = 1.68 ms and scan time = 3:44 min. The conventional sequence achieved TE = 2.9 ms and scan time = 5:23 min. In subjects with aortic stenosis, we also compared both MRI methods with Doppler ultrasound (US) in the measurement of peak velocity, time to peak systolic velocity, and eject time. Bland-Altman analysis revealed that, when comparing peak velocities, the discrepancy between Doppler US and 4D spiral flow was significantly less than the discrepancy between Doppler and 4D Cartesian flow (2.75 cm/s vs. 10.25 cm/s), whereas the two MR methods were comparable (−5.75 s vs. −6 s) for time to peak. However, for the estimation of eject time, relative to Doppler US, the discrepancy for 4D conventional flow was smaller than that of 4D spiral flow (−16.25 s vs. −20 s).

Conclusion: Relative to conventional 4D flow, 4D spiral flow achieves substantial reductions in both the TE and scan times; therefore, utility for it should be sought in a variety of in vivo and complex flow imaging applications.

Keywords

Phase-Contrast MRI; 4D flow MRI; non-Cartesian trajectories; spiral acquisition; stenotic flow

INTRODUCTION

Four-dimensional (4D) flow MRI is a relatively recent development in phase contrast MRI, which provides time-resolved 3D velocity field in a dynamic volume (1–4). This technique provides more anatomical information and comprehensive assessment of blood flow and hemodynamics. Four-dimensional flow imaging is a time-resolved 3-D k-space gated acquisition in which an additional phase-encoding is required in the third dimension. This is to be compared to 3D flow MRI, which requires three separate scans to reveal each component of 3D flow velocities. A major impediment in the application of 4D flow MRI has been the relatively long scan times, requiring the patient to remain motionless, at times on the order of several min. The scan time becomes even more prohibitive in free breathing studies in which the application of navigator gating is required, leading to increased scan times that are up to 10 min to 20 min—the total scan time being determined by the patients' specific breathing pattern.

A number of approaches have been adopted to reduce scan times. One approach for the reduction of scan times in general, and 4D flow in particular, is based on parallel imaging methods such as sensitivity encoding (SENSE) or generalized autocalibrating partially parallel acquisitions (GRAPPA) (5,6). In intracardiac 4D flow imaging with SENSE (5), typical scan parameters for 4D flow were: acceleration factor = 2, echo time/repetition time [TE/TR] = 3.7/6.3 ms temporal resolution 50 to 55 ms, spatial resolution = 3*3*3 mm^3, mean matrix size of 83*83*48, and an acquisition time of 22.5 min (7). For accelerated scans with GRAPPA in 4D flow imaging of the aorta (8), typical scan parameters were: acceleration factor = 2, TE/TR = 2.6/5 ms, temporal resolution = 40 ms, spatial resolution = 2.1*2.5*2.5 mm^3, and mean scan time = 20 min. Although powerful, the achievable acceleration factors leading to acceptable signal-to-noise ratios (SNRs) with these methods are limited. Alternative approaches to acquisition speed up include temporal encoding and k-space undersampling based on k-t BLAST (7,9). In (7), a TE/TR = 3.7/7.6 and a spatial resolution of 3*3*3 mm^3 was reported. Despite up to four-fold acceleration factors for 4D

flow acquisition, authors have reported temporal blurring and underestimation of stroke volumes.

A separate class of methods for improving scan times adopts non-Cartesian trajectories. A very successful approach has been the vastly undersampled projection approach, which benefits from shorter scan time and resolves flow-related artifacts while achieving isotropic resolutions (10). The reported imaging parameters to quantify blood flow in portal hypertension were (11): field of view (FOV) = 320*320*220 mm^3, spatial resolution = 1.3*1.3*1.3 mm^3, TE/TR = 2.1–3.2/ 6.1–7.8 ms, and scan time = 11 min. A hybrid radial-Cartesian strategy was also developed by the same group for more efficient sampling and benefiting from isotropic in-plane resolution with stack-of-stars approach in the through-plane. The reported imaging parameters in that case were: FOV = 220*220*40 mm^3, spatial resolution = 0.43*0.43*1 mm^3, TE/TR = 3.7/8 ms, and scan time = 9 min (12).

In addition to scan times, an important challenge has been the inaccuracy of conventional 4D flow in the presence of random unsteady and turbulent blood flow, often leading to signal loss and flow artifacts. Previous investigations have revealed that shorter TE decreases such errors (13). Previously, we reported on a 4D ultrashort TE (UTE) flow MRI technique (14), which permitted TEs on the order of ~1 ms.

METHODS

4D Spiral Flow MRI

In this paper, we seek to determine the efficacy of a stack-of-spirals 4D flow acquisition method to address the present challenges in 4D flow imaging. Although the achieved TEs with 4D spiral are longer than those reported in (14), they are shorter than those achievable with conventional 4D flow imaging. Furthermore, owing to the adoption of a stack-of-spirals k-space trajectory, significant savings in scan times are attained.

However, spiral readouts in phase contrast MRI generally are more sensitive to system imperfections, radio frequency, and B0 inhomogeneities. Advances in MRI hardware, including shielded gradients and eddy-current compensation techniques, have mitigated but not fully addressed the deviation between the theoretical trajectory and the actual trajectory. In the literature, methods have been proposed to more effectively correct the trajectory delays (15,16).

Pulse Sequence

Figures 1a and 1b show the schematic of a 4-point balanced Hadamard (17) 4D flow with conventional and spiral readouts that were utilized for MRI flow data collection. The 4D spiral sequence, which combines the refocusing lobe of the slice select gradient with the bipolar velocity encoding gradient, has four parts—each lasting for one TR and leading to minimum temporal resolution of 4*TR. As shown in the figure, the pulse sequence consists of flow encoding in the *z*, *y*, and *x* directions. The sequence implementations were all based on minimum TE velocity encoding (18). To avoid the off-resonance artifacts in the outer regions of k-space, interleaved spiral arms were utilized (19). Short repetition time in interleaved spiral acquisitions permits acquisition of more than one interleave in each

cardiac cycle and still maintains a reasonable temporal resolution. In general, there is a tradeoff between length of interleaves to cover the k-space and temporal resolution. Using longer spiral arms will lead to a sufficient k-space coverage with a reduced number of readouts and as a result a shorter scan time, but this will be at the cost of a longer TR and poor temporal resolution and in general worse image quality due to off-resonance effects. To achieve a better temporal resolution, many short spiral interleaves could be used (at the cost of a longer scan time). Other advantages of interleaved spiral arms include higher sampling density at the center of k-space, which will increase the SNR (at the cost of increased blurring due to subsampling the outer regions of k-space) (20,21).

In Vitro Stenotic Flow Phantom Circuit

Experiments were carried out using a closed-loop flow system (Supp. Fig. S1). A MR-compatible, computer-controlled pump (LB Pump; LB Technology LLC, Louisville, KY) was used with the capability to program user-defined flow waveforms. An idealized rigid model of axi-symmetric Gaussian shape stenosis was machined from transparent acrylic using conventional computer numerical-control machining methods with 87% area occlusion. The stenosis diameter narrowed from 25.4 mm at the inlet to 9.04 mm at the throat. A blood-mimicking solution of 60% water and 40% glycerol was used in the experiments. The viscosity of the solution utilized in the flow circuit was measured to be 0.0043 Pascal s at 68°F. The density of the solution was 1,035 kg/m3.

In Vitro Imaging Protocol

Imaging was performed on a Philips Achieva 1.5 Tesla (T) scanner (Philips Healthcare, Best, NL) using an eight-element SENSE knee coil. The gradient strength of 21 mT/m and a slew rate of 100 T/m/s were used for both conventional 4D flow and 4D spiral flow sequences. These are the values for conventional clinical acquisitions. Although the scanner is capable of achieving higher gradient strengths and slew rates (on the Philips Achieva 1.5T scanner, 33 mT/m, 180 T/m/s), the aforementioned values strike a balance between accurate flow measurement and eddy current-induced phase errors.

The imaging volume covered 60 mm of phantom, including 15 mm proximal and 45 mm distal to the stenosis. The center of the knee coil and the isocenter of the scanner were positioned 15 mm distal to the throat of the stenosis. Table 1 summarizes the imaging parameters for conventional 4D flow and 4D spiral flow acquisitions with 12, 24, and 36 interleaves for Q = 50 ml/s and 150 ml/s steady, as well as Qmax = 50 ml/s and 150 ml/s pulsatile flow experiments that were performed. The FOV, spatial resolution, flip angle, matrix size, and number of signal averages were kept the same for all experiments. For pulsatile flow acquisitions, the prescribed flow waveform at the pump is displayed in Supporting Figure S2. Electrocardiogram triggering from the pump was used, and 15 images were acquired in each cycle.

Table 1 shows Reynolds numbers, Velocity encoding parameter (Venc), TE, and TR for steady and pulsatile flow experiments for both the conventional 4D flow and 4D spiral acquisitions at the two flow rates considered. In Table 1, Reynolds number is a dimensionless number that describes the ratio of inertial to viscous forces in the flow

$$Re = \frac{\rho v D}{\mu}, \quad [1]$$

where ρ is the density of the fluid (kg/m^3), v is the mean velocity of the object relative to the fluid (m/s), D is the diameter of the tube (m), and μ is the dynamic viscosity of the fluid (kg/[ms]). A Reynolds number above 2,000 is typically considered to be in the turbulent flow regime, whereas a Reynolds number below 1,000 is in the laminar regime.

The two flow rates of 50 ml/s and 150 ml/s that were considered are associated with Reynolds numbers of 618 and 1,854 at the inlet and 1,711 and 5,134 at throat of stenosis (Table 1). These Reynolds numbers cover most Reynolds numbers that are encountered in human circulation, except perhaps flow, through a severe aortic valvular stenosis.

Analysis of In Vitro Data

All image postprocessings were performed using in-house developed software in MATLAB (The MathWorks, Natick, MA). To compute flow waveforms, velocity data were manually segmented in each axial slice based on a circular mask, with a predefined diameter in in-house software developed in MATLAB. To reduce the effect of partial volume effect, pixels having less than 50% area inside the region of interest (ROI) were excluded from flow calculation analyses. Flow in each cross section results from summation of all through-plane velocity components for that slice. GTFlow (Gyrotools, Zurich, Switzerland), a dedicated visualization software, was used to visualize flow velocities from multidimensional phase-contrast velocity images.

To reduce the phase errors, the image of flow-off acquisition with identical imaging parameters were subtracted from the phase image of flow-on acquisitions for all 4D flow acquisitions. A comparison of analysis of flow images between 4D spiral flow and conventional 4D flow for Q = 50 ml/s and Q = 0 ml/s steady flow is included in Supporting Figure S3. As can be observed from the flow-off spiral scan plot in this figure, when we are away from the isocenter, the phase errors for the spiral scan increase. This suggests placement of the ROI at the isocenter in order to reduce errors due to system imperfections.

Quantitative Comparison of In Vitro Flows

We used the relative root mean squared error (RRMSE) to compare flow waveforms measured with conventional 4D flow at locations proximal to the throat of the stenosis, with flow measurements from conventional 4D flow and/or 4D spiral flow at distal locations. It should be noted that we used the measurements from conventional 4D flow as the reference gold standard. To reduce noise, we used the mean flow waveforms in three slices proximal to stenosis using conventional 4D flow acquisition as the reference flow measurement. The reason why proximal slices were utilized in calculation of the reference flow waveform is because at higher flow rates and at locations distal to the throat of the stenosis, signal dephasing occurs, which corrupts the measurements. Furthermore, we have a completely rigid phantom. Therefore, setting aside measurement errors, the flow waveform must be identical at different locations along the length of the phantom.

The RRMSE metric has the following form:

$$\mathrm{RRMSE} = 100\,\% \times \sqrt{\frac{\sum_t \sum_n (Q_{\mathrm{sp/conv}}(n,t) - \mathrm{Q_{inlet}}(n,t))^2}{\sum_t \sum_n (\mathrm{Q_{inlet}}(n,t))^2}}, \quad [2]$$

where $\mathrm{Q_{inlet}}$ is inlet reference flow measured with conventional 4D flow by averaging the flow in three slices proximal to the stenotic narrowing, and $\mathrm{Q_{sp/conv}}$ is the measured flow using the 4D spiral acquisition or the conventional 4D flow acquisition. The index t represents cine slice numbers acquired in time for the pulsatile acquisitions in which $t = 1$ is the first phase and $t = 15$ is the last phase of the cardiac cycle. However, for the case of steady flow acquisitions, $t = 1$. n is the slice position number along the phantom length in which $n = 1$ is the first collected slice and $n = 20$ is the last collected slice. Note that $n = 5$ is the slice located at the center of the stenosis, slice $n = 1$ is located at $z = -12$ mm, and slice $n = 20$ is located at $z = +45$ mm. Supporting Figure S1c shows a schematic geometry of the phantom and different regions of FOV for data analyses.

In Vivo Imaging Protocol

The study was approved by the institutional review board at the Veterans Affairs Medical Center in Louisville, Kentucky. Five healthy male volunteers (average age = 32.6 years old, average weight = 71.4 kg) and four patients with mild to moderate aortic stenosis (average age = 68.5 years old; average weight = 95.6 kg) were recruited to the study. All subjects underwent both conventional 4D flow and 4D spiral flow MRI exams back to back. Cardiac and respiratory gating was undertaken. The scan parameters for the two sequences were TE/TR = 2.9/5.1 ms (conventional 4D flow); TE/TR = 1.68/7.7 ms (4D spiral); Venc = 400 cm/s in all three flow directions; flip angle = 6; in-plane spatial resolution = 2.5*2.5 mm^2; FOV = 200*200*50 mm^3; and slice thickness = 5 mm. For the 4D spiral sequence, 36 interleaves with 4 ms readout each were adopted. It should be noted that, although the 24-interleave sequence leads to satisfactory results for the phantom studies (e.g., see Figure 2), for in vivo studies, a larger number of interleaves was required due to the larger size of the FOV (100 × 100 mm^2 vs. 200 × 200 mm^2). Additionally, to permit direct comparison of hemodynamics across both MR modalities for both 4D scans and for all studies, we fixed the number of phases to 15. The scan time for conventional 4D flow was 5:23 min, and for 4D spiral flow it was 3:44 min. However, due to the application of navigator gating and depending on patient's breathing pattern, each scan took up to three times longer.

RESULTS

Steady Flows: Qualitative Comparison of Velocity Profiles

Two-Way Comparisons—Figure 3a shows velocity-vector profiles for Q = 50 ml/s for conventional 4D and 4D spiral acquisitions with 12, 24, and 36 spiral interleaves. All four acquisitions measured the flow with similar accuracy; however, the scan time was much shorter for the 4D spiral acquisitions. Moreover, 4D spiral acquisitions permitted echo times on the order of 2 ms as compared to 3.6 ms for the conventional 4D acquisition. In the case of higher flow rates, for which intravoxel dephasing was present due to turbulence and flow jet, 4D spiral flow was able to obtain better velocity profiles as compared to the conventional

acquisition. Figure 3b demonstrates velocity vector profiles at Q = 150 ml/s for conventional 4D and 4D spiral acquisitions. Assuming a sufficient number of spiral interleaves to avoid streaking artifacts, the spiral acquisitions generally lead to improved visualization of velocity profiles due to shorter TEs. The recirculation zone (eddy flow), distal to the throat of the stenosis, was observable in all acquisitions for the low flow rate of 50 ml/s. However, in the high flow rate of 150 ml/s, 4D spiral flow acquisitions led to better visualization of the recirculation zone.

The streaking artifact in the spiral acquisition becomes prominent when the k-space is undersampled. Supporting Figure S4a illustrates the streaking artifacts in an axial phantom image with 12 interleaves, whereas Supporting Figures S4b,c illustrate that increasing the number of interleaves to 24 and 36 results in less streaking artifact.

Figures 2a and b display a magnitude of spatially resolved 3D velocities for Q = 50 ml/s at the midsagittal slice location, as well as an axial location at 21 mm distal to the throat of the stenosis for conventional 4D flow (Fig. 2a) and 4D spiral flow with 24 spiral interleaves (Fig. 2b). There is no noticeable difference between these visualizations at Q = 50 ml/s. Figures 2c and d display magnitude of spatially resolved 3D velocities for Q = 150 ml/s at the midsagittal slice location, as well as an axial slice at 21 mm distal to the throat of the stenosis for conventional 4D flow (Fig. 2c) and 4D spiral flow with 24 spiral interleaves (Fig. 2d). Results from conventional 4D flow at this higher flow rate show artifacts at distal locations. However, there is a noticeable improvement when utilizing 4D spiral acquisition. This is primarily due to the shorter achievable TE of the spiral acquisition (TE = 1.57 ms), which is to be compared with the longer TE time (TE = 3.2 ms) for conventional 4D flow.

Three-Way Comparisons—In addition to testing against 4D conventional flow, 4D spiral was also tested against 4D radial UTE method (14), which permits substantially reduced echo times. We tested all three sequences for identical FOVs at a steady flow rate of 300 ml/s: conventional 4D flow with TE = 3.1 ms, 4D spiral flow with 24 interleaves with TE = 1.51 ms, and 4D UTE flow with 75% k-space sampling and with TE = 1.10 ms—all remaining imaging parameters (including Venc = 500 cm/s) remaining identical. As displayed in Figure 4, flow artifacts resulting from intravoxel dephasing seen distal to the throat of the stenosis directly correlate with TE. Whereas conventional 4D flow lead to significant flow artifacts, 4D spiral flow had improved performance. However, 4D-UTE flow's performance was best and was able to completely resolve the artifacts encountered with conventional 4D flow. Scan times for 4D spiral flow was best with scan times for each of the three acquisitions as follows: 4D conventional flow: 51 s, 4D spiral flow: 38 s, 4D UTE flow: 69 s.

Steady Flows: Quantitative Flow Comparison Results

Table 2 shows scan times and RRMSE for both conventional 4D flow and 4D spiral flow acquisitions with 12, 24, and 36 interleaves for Q = 50 ml/s and 150 ml/s steady flow rates. At distal locations, it is evident that as the flow rate increases, the performance of the conventional acquisition degrades more severely. We believe that this is due to increased spin dephasing, which occurs at high velocities. For the spiral acquisition at distal locations,

the deterioration in performance is less pronounced than the conventional acquisition, and more specifically for the 24 and 36 spiral arm acquisitions, which do not suffer from streaking artifacts. This is due to the smaller achievable TEs for the spiral acquisitions. Indeed, as was observed in the three-way comparisons, as the flow rate was further increased, the performance of the conventional 4D acquisition significantly worsened.

In terms of scan time, the 4D spiral acquisition outperformed conventional 4D flow for all flow rates and flow regimes. As may be observed in Table 2, at Q = 50 ml/s, 4D spiral flow resulted in 70%, 34%, and 16% reduction in scan time for each of 12, 24, and 36 spiral interleave acquisitions, respectively. At Q = 150 ml/s, 65%, 25%, and 6% reduction in scan time were achieved relative to conventional 4D flow.

Pulsatile Flow Experiments

Flow assessment and quantification was performed in the same phantom under pulsatile flow using both conventional 4D flow and 4D spiral flow acquisition. The peak of the pulsatile flow waveform shown in Supporting Figure S2 was adjusted to the value of the steady flow experiments described previously (i.e., Qmax = 50 and 150 ml/s) and prescribed at the pump. However, it should be noted that due to the compliance of tubes and flow connectors relative to the programmed flow waveform shown in Supporting Figure S2, the measured flow waveform is indeed damped. Supporting Figure S5 displays the averaged damped measured flow waveforms with conventional Cartesian acquisition at three proximal slices and for two flow experiments with peak flow rate Qmax = 50 ml/s and Qmax = 150 ml/s. It is observed that peak of flow waveforms were damped to about 55% of prescribed value at the pump due to compliance of tubes in the flow system.

Qualitative Pulsatile-Flow Comparison Results

As stated previously, the flow waveform must remain identical at all axial cross sections of the phantom. In order to remove the effect of measurement noise and accentuate the signal dephasing effects that occur distal to the throat of the stenosis, the flow waveforms from both conventional 4D flow and 4D spiral flow were measured from 12 axial slices distal to the stenosis and then were averaged. Figure 5 reports the results. At Qmax = 50 ml/s, there was good agreement between conventional 4D flow and 4D spiral flow techniques; however, at Qmax = 150 ml/s, there was slightly more agreement between 4D spiral 36 and reference flow than that of conventional 4D flow and reference flow. We believe that this discrepancy was due to the longer TE in conventional 4D flow relative to the 4D spiral flow, which in turn resulted in more spin dephasing.

Quantitative Pulsatile-Flow Comparison Results

Two-Way Comparisons—Table 2 also shows the scan time and the measured RRMSE between reference flow waveform and conventional 4D flow and 4D spiral flow for different number of interleaves under two pulsatile flow waveforms (Qmax = 50 ml/s, 150 ml/s).

For the flow rates considered, the performance of the 4D spiral was close to conventional 4D flow. In the high flow-rate case of 150 ml/s, spiral 36 achieved the same RRMSE as the Cartesian acquisition. Spiral 12, spiral 24, and spiral 36 achieved scan times of 5:14 min,

10:26 min, and 7:50 min, respectively, as compared to conventional Cartesian, which had a scan time of 14:20 min. This translates to 63%, 28%, and 45% reduction in scan times for each of the spiral 12, spiral 24, and spiral 36 relative to the conventional 4D flow for both flow rates.

Note that, despite having more spiral interleaves, spiral 36 had a shorter scan time than spiral 24. The reason for this apparent discrepancy is that the readout time for spiral 36 was smaller (4 ms) versus spiral 24 (6 ms) and spiral 12 (9 ms). The smaller readout time resulted in the possibility for the acquisition of two (as opposed to one) k-space arms per R-wave and reduced total acquisition time. We had the choice of leaving the segmentation factor as 1, but this would have doubled the total scan time for spiral 36.

Human Studies Results

Figure 6 shows an example of in vivo studies in a normal volunteer and in a subject with moderate aortic stenosis (note that (22) include many more visualization results, which due to space limitations were not included here). The left column of Figure 6 shows systolic velocity profile in a normal volunteer from conventional 4D flow (top) and 4D spiral flow (middle). The corresponding flow waveforms versus cardiac time at 15 mm distal to the aortic valve using both conventional 4D flow MRI (blue plot) and 4D spiral flow MRI (red plot) are superimposed in the panel in the bottom. The right column of Figure 6 shows systolic velocity profile in a subject with aortic stenosis from conventional 4D flow (top) and 4D spiral flow (middle). The corresponding flow waveforms versus cardiac time at 15 mm distal to the aortic valve using both conventional 4D flow MRI (blue plot) and 4D spiral flow MRI (red plot) are superimposed in the panel in the bottom. Qualitatively, there is good correlation between the two MRI techniques in flow measurement, though 4D spiral flow acquired the data with a 30% reduction in scan time.

Table 3 reports on a comparison of several flow indices between the 4D spiral acquisitions and conventional 4D acquisition in the 9 subjects (5 normal subjects and 4 patients suffering from aortic stenosis). Note that for the case of the patients, we report the corresponding Doppler US-derived indices, which are commonly used in echo-cardiographic studies. The indices included the peak elocity, time to peak, and eject time, which were derived from the different acquisition methods. Peak velocity is the peak systolic velocity measured during the cardiac cycle by inspecting all slices distal to the aortic valve. Time to peak is the time from the onset of the R-wave to the peak measureable systolic velocity. Eject time is the effective systolic time measured between the onset of the R-wave to the closure of the aortic valve, as determined from rapid decline of output flow distal to the valve.

Table 4 displays results of Bland-Altman analysis, which was performed between each MR modality and Doppler US for each of the three indices considered. Bland-Altman analysis revealed that, when comparing peak velocities, the bias between Doppler US and 4D spiral flow was significantly less than the bias between Doppler and 4D Cartesian (2.75 cm/s vs. 10.25 cm/s), whereas for time to peak, relative to Doppler US, the two MR methods were comparable (bias of −5.75 s vs. −6 s). However, for the estimation of eject time, the bias for 4D conventional flow was smaller than that of the 4D spiral flow (−16.25 s vs. −20 s).

DISCUSSION

Phantom Studies

In phantom studies of stenotic flows, results based on the RRMSE criterion for the flow rates considered revealed that, with sufficient number of interleaves, 4D spiral flow is capable of providing a level of accuracy similar to conventional 4D flow but with a 28% to 63% reduction in scan time in the case of pulsatile studies. The 4D spiral method has the added advantage of achieving a shorter TE—on the order of 44% to 51% reduction. This reduction becomes especially meaningful at high flow rates, as illustrated in Figure 4, which displays magnitude of velocities for the case of Q = 300 ml/s (leading to peak velocities under 5 m/s, velocities that could very well occur in subjects with severe aortic stenosis). As may be appreciated from this figure, there is significant deterioration of conventional 4D flow velocities compared to the spiral acquisition. Qualitative results in phantom studies revealed that both methods perform similarly for flow profile visualization; however, at higher flow rates, 4D spiral showed better performance in visualization of jet flows distal to the occlusion relative to conventional 4D flow.

From the three-way comparison of 4D conventional, 4D UTE, and 4D spiral, it may be concluded that each of the two latter sequences address different challenges in flow imaging — 4D UTE is better suited in imaging complex flows at high Reynolds numbers; whereas 4D spiral is well suited to imaging moderately high flows, although with the clear advantage of reduced scan times. At high flow rates, 4D UTE flow is the most accurate due to shorter TEs. The quality degrades somewhat for the 4D spiral flow and significantly for the 4D conventional flow.

A limitation of this study is that, in the comparisons presented in Table 2, we made use of conventional 4D flow measurements at locations proximal to the throat of the stenosis as the reference ground truth, and we subsequently used this in calculating the RRMSE between flow measured with the conventional 4D flow or 4D spiral flow at other regions of the phantom. This approach may have caused a bias in favor of the conventional 4D flow acquisition in our reported RRMSE values, though the bias is not in the measurement but instead in the comparisons. There are other independent approaches based on Doppler US (23), particle image velocimetry (24), or electromagnetic flow meters (25), though such measurements would clearly be more involved, requiring additional instrumentation.

Human Studies

Results indicate that 4D spiral is capable of providing the same level of accuracy in flow measurement as in conventional 4D flow MRI for imaging the flow through the aortic valve but relative to conventional 4D flow, on average with a 30% reduction in scan time and 45% reduction in echo time. 4D spiral was also able to achieve a TE of 1.68 ms versus 2.9 ms for conventional 4D flow MRI, permitting less signal dephasing distal to occlusions. One limitation for application of the method in vivo is the clear lack of availability of a “flow-off” phase image for the purpose of phase correction. As may be gathered by examining Supporting Figure S3, phase errors increase in off-center slices. Therefore, for the in vivo

situation, placing the region of interest at the isocenter of the magnet should reduce these errors.

Relation to Previous Work

Recently, Sigfridsson et al. (26) also proposed a spiral 4D flow MRI method. Their method achieved TE on the order of 3.5 ms in spiral acquisition vs 3.4 ms for the conventional Cartesian acquisition. In order to avoid off-resonance artifact due to fat encountered in long readout spiral acquisitions, Sigfridsson et al. employ a 1–1 water-only excitation, which lengthens the TE in their approach. However, use of short readout interleaves can also resolve off-resonance artifacts (26,27), which is the method adopted in our approach. As with Sigfridsson et al.'s work, we adopt a spiral k-space trajectory; however, we are able to improve on achieved TEs by combining the refocusing lobe of the slice select and flow encoding gradients.

Other methods that have adopted a stack of spirals for 4D flow acquisitions include Nilsson et al. (28). In this work, which was tested under steady-flow phantom experiments, velocities from MRI were compared to CFD simulations. Compared to this method, we adopt Hadamard velocity encoding, which should further improve SNR and accuracy of velocity measurements. Janiczek et al. (29) performed 4D flow MRI using a stack of spirals for flow imaging in the aortic arch of rodents and subsequently used this information to derive wall shear stress. For rodent imaging, they point out that the unique flow environment of the mouse precludes the use of conventional 4D flow imaging, which can lead to substantial flow artifacts and poor SNR.

CONCLUSION

The applicability of the 4D spiral acquisition has been shown through both phantom and in vivo studies. 4D spiral flow benefits from reduced scan times as well as reduced TEs, which should lead to improved flow assessments, primarily in regions distal to occlusions and at moderately high flow rates. In the subjects studied, it was observed that the peak velocities derived from 4D spiral flow consistently had higher values relative to conventional 4D flow. This can be due to the longer echo times in the conventional 4D flow acquisition, leading to underestimation of high velocities at peak systolic times relative to 4D spiral acquisitions. In addition, relative to Doppler US in the four patients that were studied, on average, 4D spiral flow slightly underestimated peak systolic velocities, whereas 4D conventional flow more significantly underestimated the peak systolic velocities.

Supplementary Material

Refer to Web version on PubMed Central for supplementary material.

Acknowledgments

Grant sponsor: This work was supported in part by the National Science Foundation (grant 0730467) and by an Innovative Translational Research Award from the Clinical and Translational Research Program of the University of Louisville to Amir Amini, Ph.D.

REFERENCES

1. Wigstrom L, Sjoqvist L, Wranne B. Temporally resolved 3D phase-contrast imaging. Magn Reson Med 1996;36:800–803. [PubMed: 8916033]
2. Bley TA, Johnson KM, Francois CJ, Reeder SB, Schiebler ML, B RL, Consigny D, Grist TM, Wieben O. Noninvasive assessment of transstenotic pressure gradients in porcine renal artery stenoses by using vastly undersampled phase-contrast MR angiography. Radiology 2011;261:266–273. [PubMed: 21813739]
3. Markl M, Frydrychowicz A, Kozerke S, Hope M, Wieben O. 4D flow MRI. J Magn Reson Imaging 2012;36:1015–1036. [PubMed: 23090914]
4. Hope MD, Meadows AK, Hope TA, Ordovas KG, Saloner D, Reddy GP, Alley MT, Higgins CB. Clinical evaluation of aortic coarctation with 4D flow MR imaging. J Magn Reson Imaging 2010;31:711–718. [PubMed: 20187217]
5. Pruessmann KP, Weiger M, Scheidegger MB, Boesiger P. SENSE: sensitivity encoding for fast MRI. Magn Reson Med 1999;42:952–962. [PubMed: 10542355]
6. Griswold MA, Jakob PM, Heidemann RM, Nittka M, Jellus V, Wang J, Kiefer B, Haase A. Generalized autocalibrating partially parallel acquisitions (GRAPPA). Magn Reson Med 2002;47:1202–1210. [PubMed: 12111967]
7. Carlsson M, Toger J, Kanski M, Bloch KM, Stahlberg F, Heiberg E, Arheden H. Quantification and visualization of cardiovascular 4D velocity mapping accelerated with parallel imaging or k-t BLAST: head to head comparison and validation at 1.5 T and 3 T. J Cardiovasc Magn Reson 2011;13:55. [PubMed: 21970399]
8. Schnell S, Markl M, Entezari P, Mahadewia RJ, Semaan E, Stankovic Z, Collins J, Carr J, Jung B. k-t GRAPPA accelerated four-dimensional flow MRI in the aorta: effect on scan time, image quality, and quantification of flow and wall shear stress. Magn Reson Med 2014:72:522–533. [PubMed: 24006309]
9. Tsao J, Boesiger P, Pruessmann KP. k-t BLAST and k-t SENSE: dynamic MRI with high frame rate exploiting spatiotemporal correlations. Magn Reson Med 2003;50:1031–1042. [PubMed: 14587014]
10. Gu T, Korosec FR, Block WF, Fain SB, Turk Q, Lum D, Zhou Y, Grist TM, Haughton V, Mistretta CA. PC VIPR: a high-speed 3D phase-contrast method for flow quantification and high-resolution angiography. AJNR Am J Neuroradiol 2005;26:743–749. [PubMed: 15814915]
11. Roldan-Alzate A, Frydrychowicz A, Niespodzany EJ, Landgraf BR, Wieben O, Reeder SB. 4D MR velocity mapping using PC VIPR to quantify blood flow in portal hypertension. In Proceedings of the 19th Annual Meeting of ISMRM Meeting & Exhibition in Montreal, Quebec, Canada, 2011 p 728.
12. Kecskemeti S, Johnson K, Wu Y, Mistretta C, Turski P, Wieben O. High resolution three-dimensional cine phase contrast MRI of small intracranial aneurysms using a stack of stars k-space trajectory. J Magn Reson Imaging 2012;35:518–527. [PubMed: 22095652]
13. O'Brien KR, Gabriel RS, Greiser A, Cowan BR, Young AA, Kerr AJ. Aortic valve stenotic area calculation from phase contrast cardiovascular magnetic resonance: the importance of short echo time. J Cardiovasc Magn Reson 2009;11:49. [PubMed: 19925667]
14. Kadbi M, Negahdar M, Cha JW, Traughber M, Martin P, Stoddard MF, Amini AA. 4D UTE flow: a phase-contrast MRI technique for assessment and visualization of stenotic flows. Magn Reson Med 2015;73:939–950. [PubMed: 24604617]
15. Tan H, Meyer CH. Estimation of k-space trajectories in spiral MRI. Magn Reson Med 2009;61:1396–1404. [PubMed: 19353671]
16. Bhavsar PS, Zwart NR, Pipe JG. Fast, variable system delay correction for spiral MRI. Magn Reson Med 2014;71:773–782. [PubMed: 23508831]
17. Dumoulin CL, Souza SP, Darrow RD, Pelc NJ, Adams WJ, Ash SA. Simultaneous acquisition of phase-contrast angiograms and stationary-tissue images with Hadamard encoding of flow-induced phase shifts. J Magn Reson Imaging 1991;1:399–404. [PubMed: 1790361]

18. Bernstein MA, Shimakawa A, Pelc NJ. Minimizing TE in moment-nulled or flow-encoded two- and three-dimensional gradient-echo imaging. J Magn Reson Imaging 1992;2:583–588. [PubMed: 1392252]
19. Kadbi M, Negahdar MJ, Traughber M, Martin P, Amini AA. A fast reduced TE 4D spiral PC MRI sequence for assessment of flow and hemodynamics. In Proceedings of the 21st Annual Meeting of ISMRM Meeting & Exhibition in Salt Lake City, Utah, USA, 2013 p. 4445.
20. Nayak KS, Hu BS, Nishimura DG. Rapid quantitation of high-speed flow jets. Magn Reson Med 2003;50:366–372. [PubMed: 12876713]
21. Takahashi A, Li TQ, Stødkilde-Jørgensen H. A pulse sequence for flow evaluation based on self-refocused RF and interleaved spiral readout. J Magn Reson 1997;126:127–132. [PubMed: 9252282]
22. Negahdar M 4D Reduced TE (RTE) Spiral Phase Contrast MRI for Rapid Quantification and Visualization of Blood Flow and Hemodynamics. Louisville, KY: University of Louisville; 2014.
23. Hoppe M, Heverhagen JT, Froelich JJ, Kunisch-Hoppe M, Klose KJ, Wagner HJ. Correlation of flow velocity measurements by magnetic resonance phase contrast imaging and intravascular Doppler ultrasound. Invest Radiol 1998;33:427–432. [PubMed: 9704280]
24. van Doorne CWH, Westerweel J. Measurement of laminar, transitional and turbulent pipe flow using stereoscopic-PIV. Exp Fluids 2007;42: 259–279.
25. O'Brien KR, Cowan BR, Jain M, Stewart RA, Kerr AJ, Young AA. MRI phase contrast velocity and flow errors in turbulent stenotic jets. J Magn Reson Imaging 2008;28:210–218. [PubMed: 18581344]
26. Sigfridsson A, Petersson S, Carlhall CJ, Ebbers T. Four-dimensional flow MRI using spiral acquisition. Magn Reson Med 2012;68:1065–1073. [PubMed: 22161650]
27. Fielden SW, Meyer CH. A simple acquisition strategy to avoid off-resonance blurring in spiral imaging with redundant spiral-in/out k-space trajectories. Magn Reson Med 2014;73:704–710. [PubMed: 24604539]
28. Nilsson A, Revstedt J, Heiberg E, Stahlberg F, Bloch KM. Volumetric velocity measurements in restricted geometries using spiral sampling: a phantom study. MAGMA 2014. doi: 10.1007/s10334-014-0449-0.
29. Janiczek RL, Blackman BR, Roy RJ, Meyer CH, Acton ST, Epstein FH. Three-dimensional phase contrast angiography of the mouse aortic arch using spiral MRI. Magn Reson Med 2011;66:1382–1390. [PubMed: 21656547]

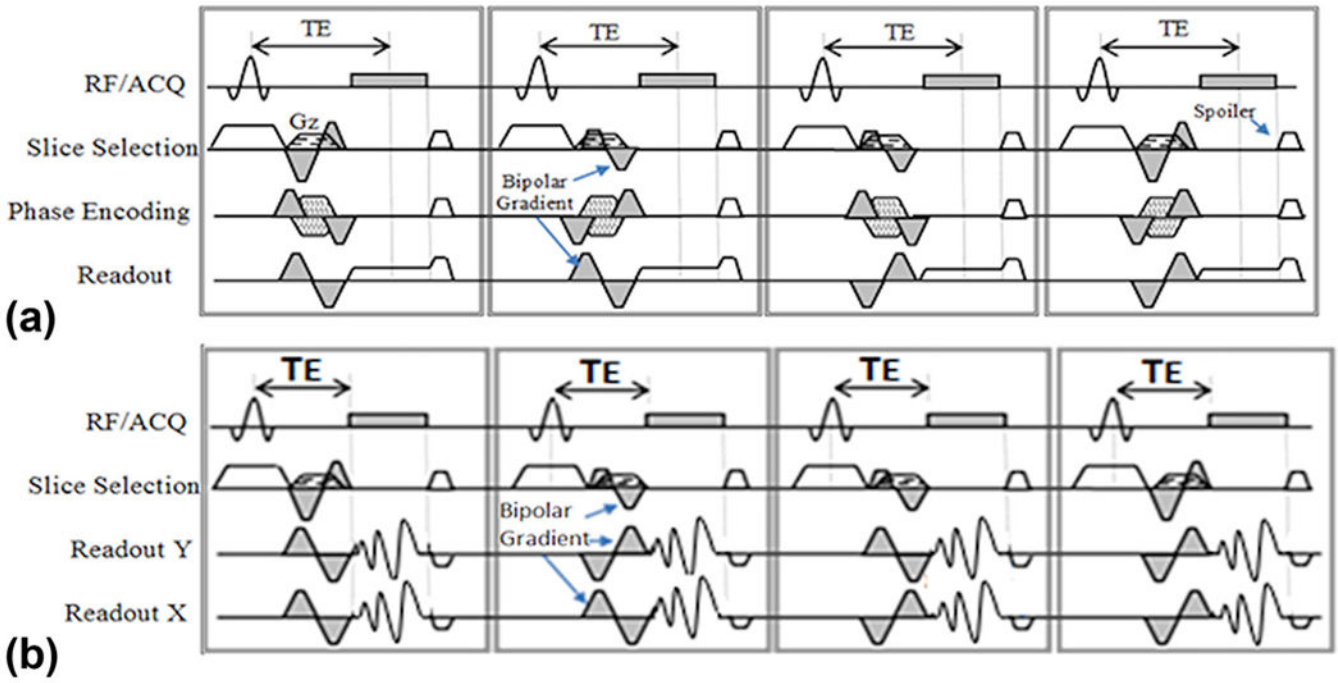

FIG. 1.

Schematic for conventional four-dimensional (4D) flow MRI (a) and 4D spiral flow (b) utilized in this paper, both with Hadamard encoding for improved signal-to-noise ratio. Gray shaded gradients indicate flow sensitive gradients in each flow direction. Arrows point to bipolar velocity-encoding gradients. ACQ, acquisition; RF, radio frequency; TE, echo time.

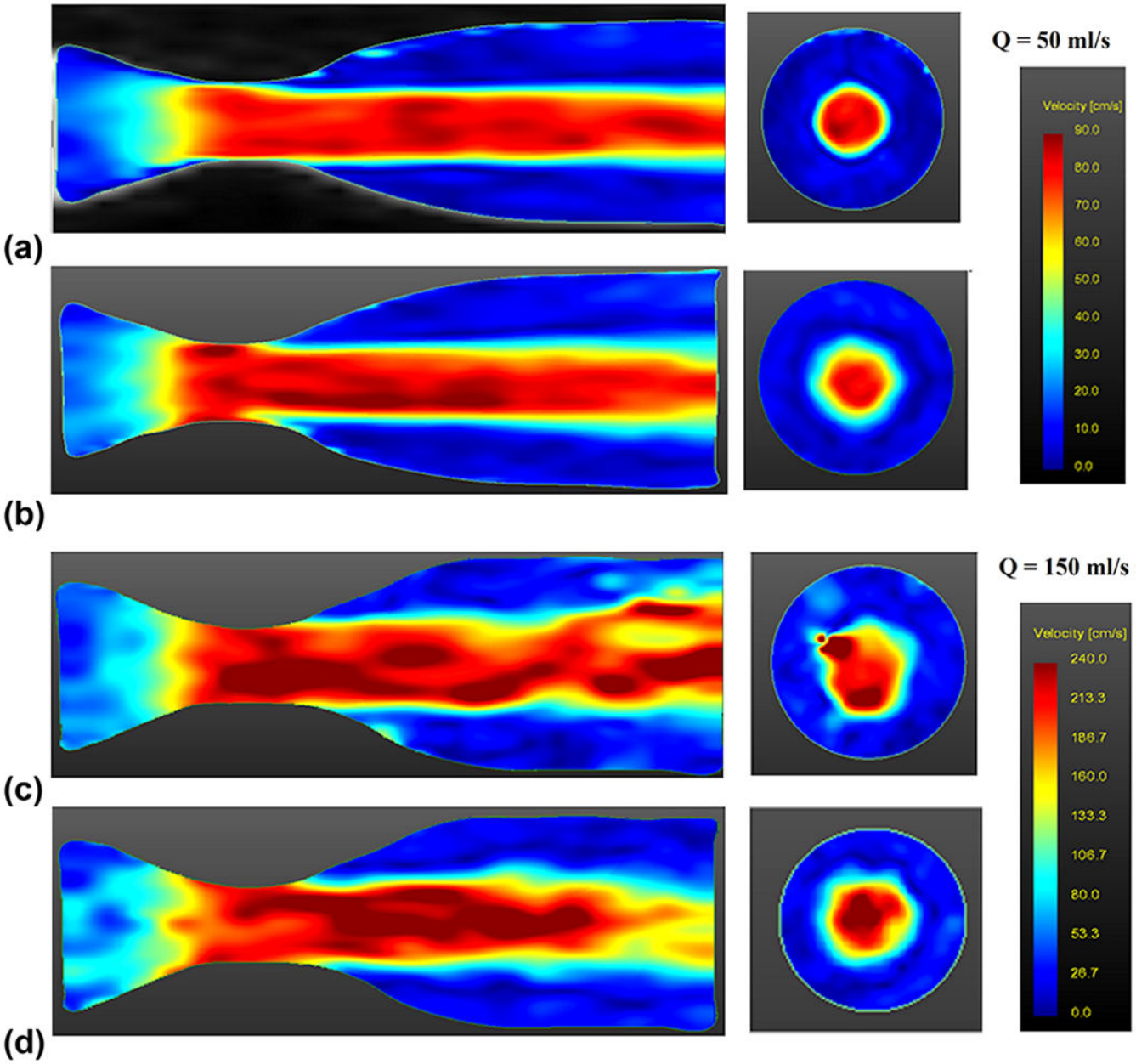

FIG. 2.

Velocity magnitude profile visualization at (a) Q = 50 ml/s steady flow for conventional four-dimensional (4D) flow acquisition, (b) Q = 50 ml/s steady flow for 4D spiral acquisition with 24 interleaves, (c) Q = 150 ml/s steady flow for conventional 4D flow, and (d) Q = 150 ml/s steady flow for 4D spiral acquisition with 24 interleaves. All visualizations on left are from midsagittal slice, and all visualizations on right are from an axial slice located at 21 mm distal to throat of stenosis.

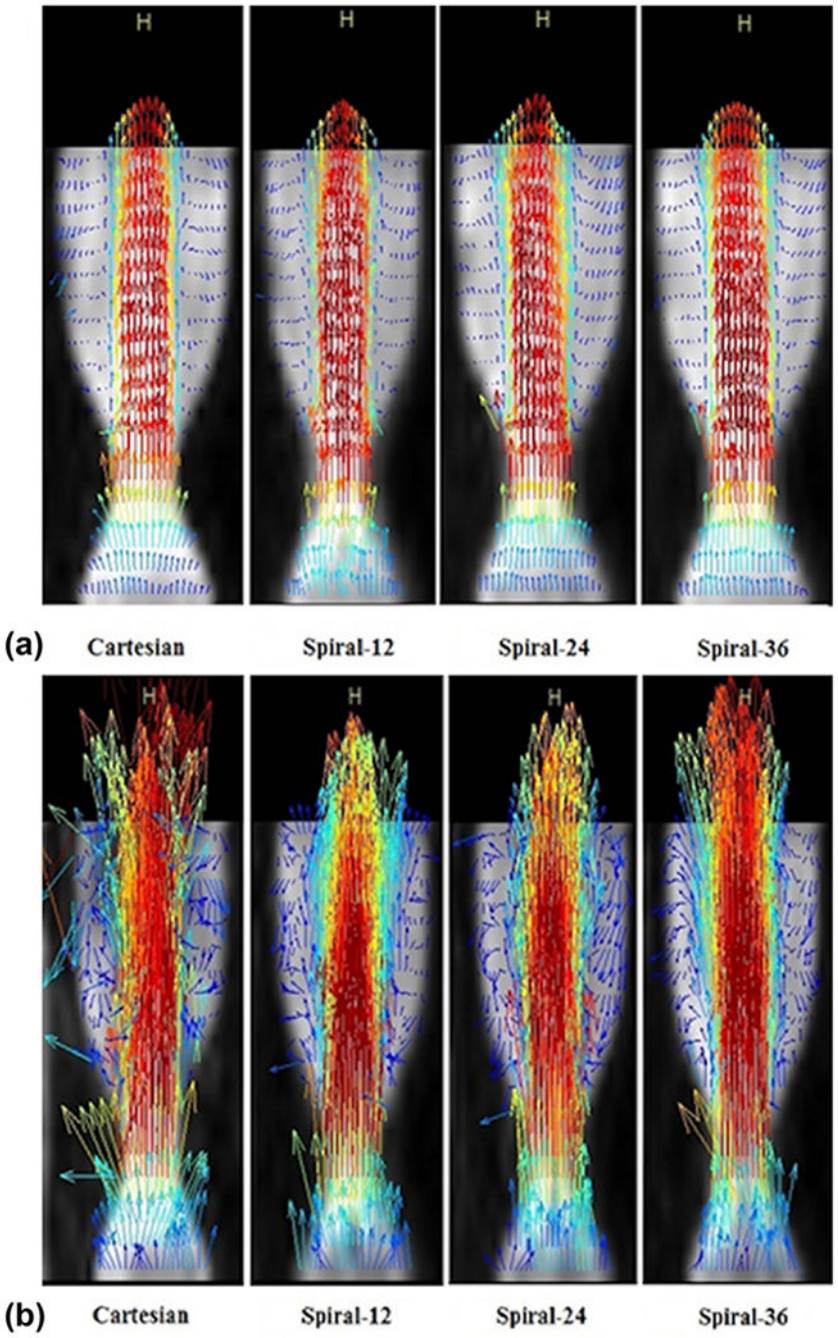

FIG. 3.

(a) Sagittal view of velocity vector profile visualization at Q = 50 ml/s steady flow for conventional four-dimensional (4D) and 4D spiral acquisitions. (b) Sagittal view of visualization of velocity vectors at Q = 150 ml/s steady flow for conventional 4D and 4D spiral acquisitions. Flow is from bottom toward top.

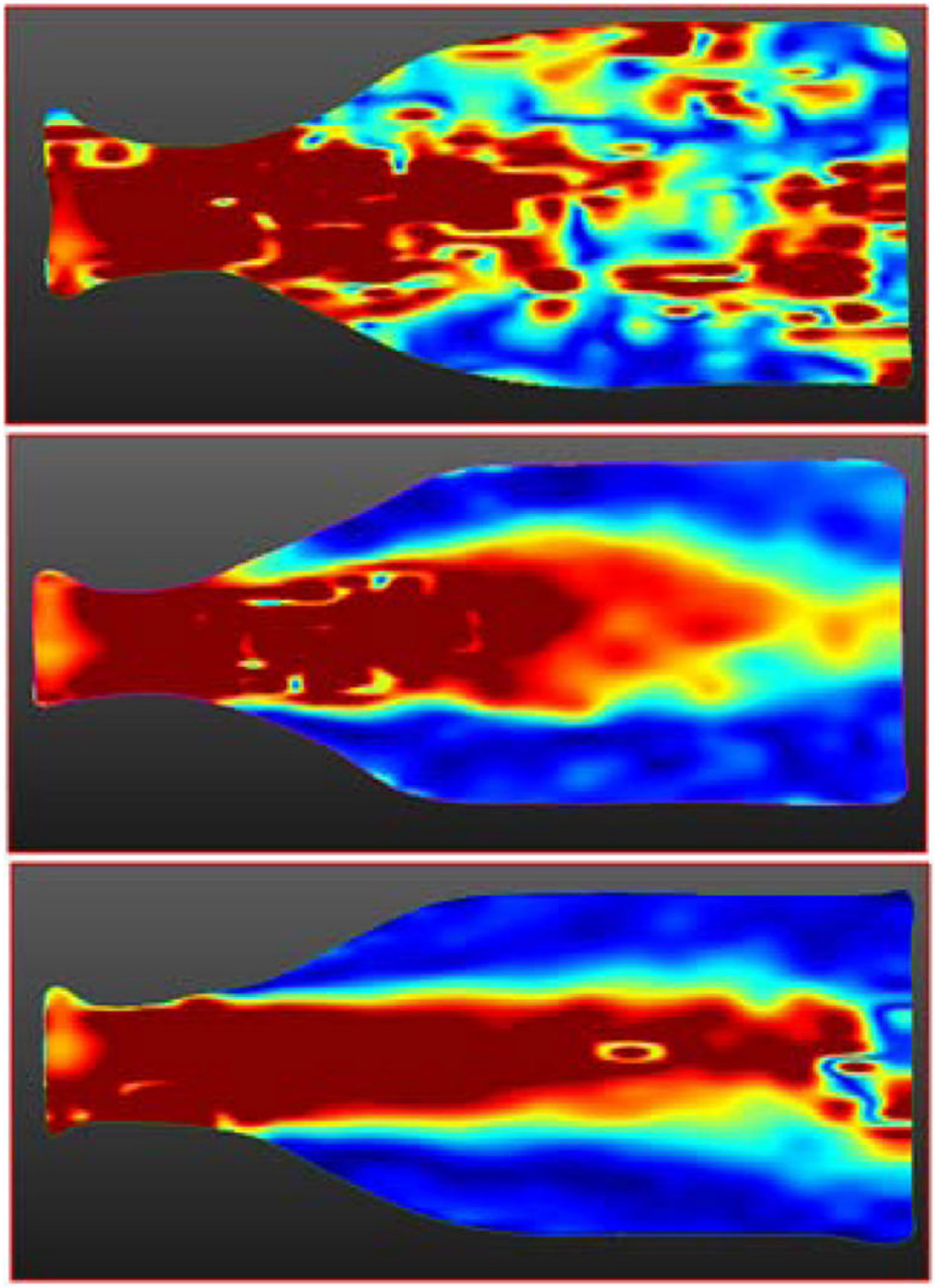

FIG. 4.

Flow artifacts visualized in a sagittal velocity magnitude image for Q = 300 ml/s steady flow. (a) Conventional four-dimensional (4D) flow with echo time (TE) = 3.1, (b) 4D spiral flow with TE = 1.51, and (c) 4D ultrashort TE (UTE) flow with TE = 1.10. As can be seen, flow artifacts resulting from intravoxel dephasing directly correlate with TE. Conventional 4D flow leads to significant flow artifacts. 4D spiral flow has improved performance relative to conventional 4D flow. 4D UTE flow is able to completely resolve flow artifacts encountered with conventional 4D flow.

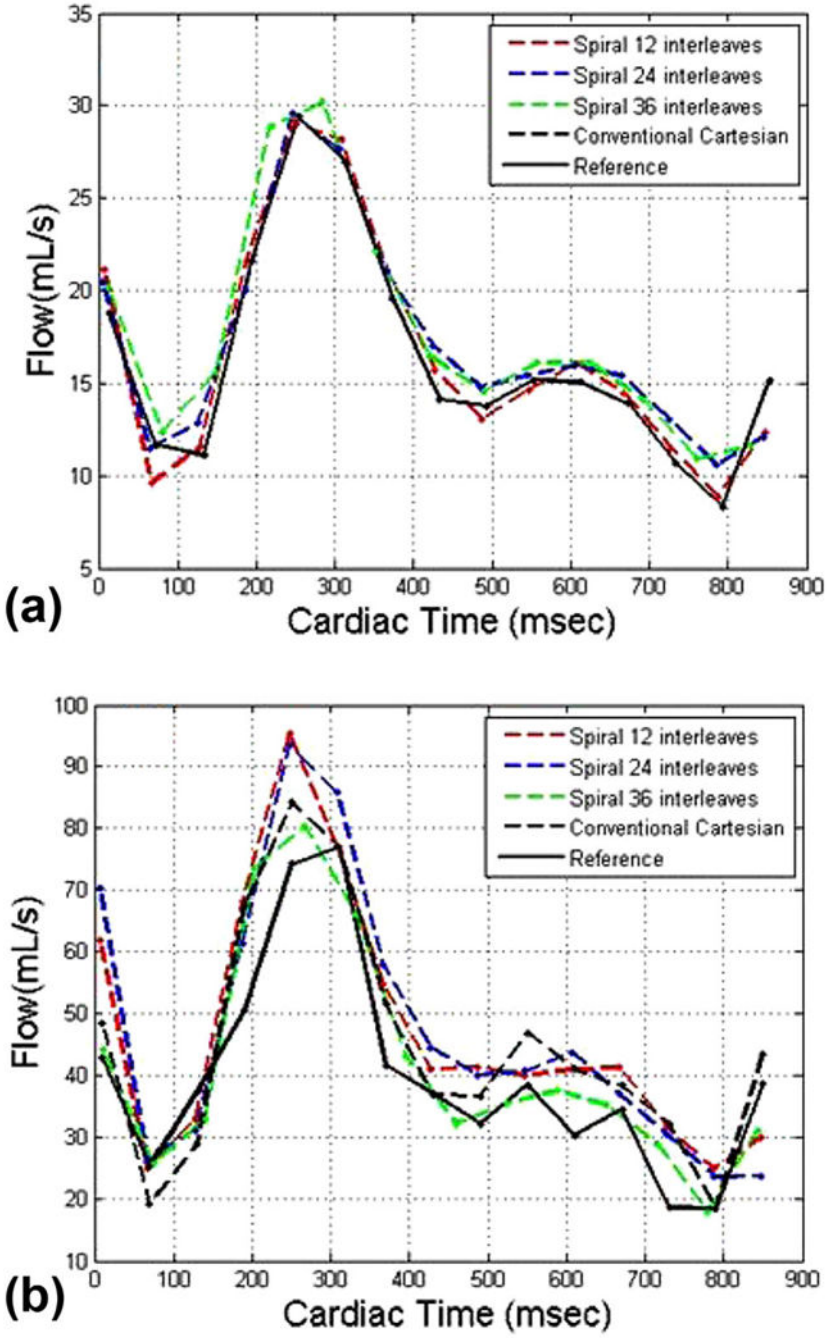

FIG. 5.

Mean flow waveform in 12 slices distal to stenosis for both four-dimensional (4D) conventional and 4D spiral acquisitions with (a) Qmax = 50 ml/s and (b) Qmax = 150 ml/s.

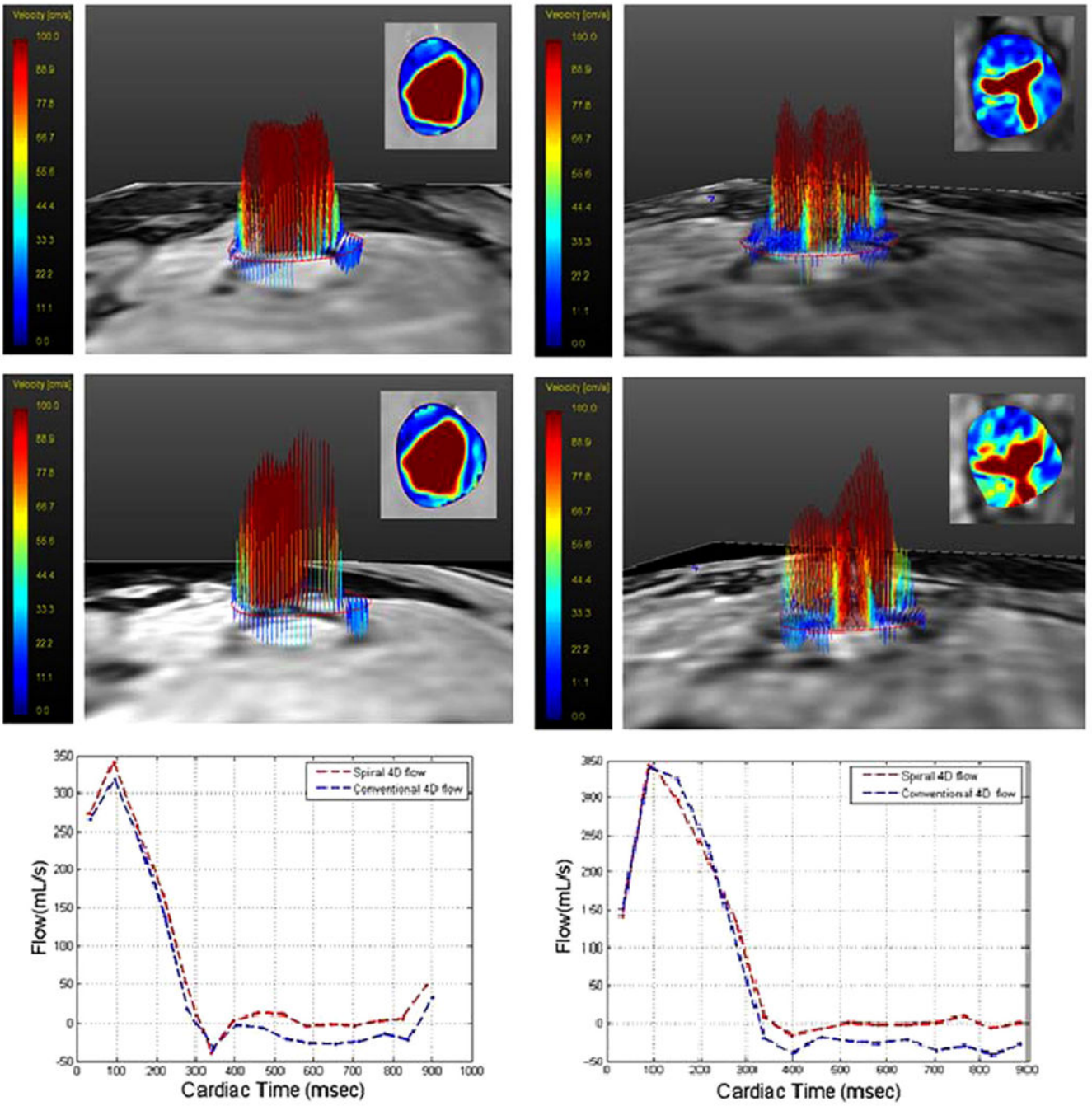

FIG. 6.

Left: Velocity profiles in both three-dimensional (3D) and 2D views (inset) for flow at level of aortic valve at peak systole in healthy volunteer using conventional 4D flow (top) and 4D spiral flow (middle). Flow waveform versus time at 15 mm distal to aortic valve in normal volunteer subject, using conventional 4D flow (blue plot) and 4D spiral flow (red plot) (bottom). Right: Velocity profiles in both 3D and 2D views (inset) for flow at level of aortic valve at peak systole in a subject with aortic stenosis using conventional 4D flow (top) and 4D spiral flow (middle). Flow waveform versus time at 15 mm distal to aortic valve in

subject with aortic stenosis, using conventional 4D flow (blue plot) and 4D spiral flow (red plot) (bottom).

Table 1

Scan Parameters for Conventional 4D Flow and 4D Spiral Acquisition With 12, 24, and 36 Interleaves for Steady and Pulsatile Flow Phantom Studies at Qmax = 50 ml/s and 150 ml/s Flow Rates.[a]

		Q = 50 ml/s	Q = 150 ml/s
Reynolds Number (equation [1])	Inlet	618	1,854
	Throat	1,711	5,134
Venc (cm/s)		150	450
Field of View (mm)		100*100*60	100*100*60
Resolution (mm)		1.5*1.5*3	1.5*1.5*3
Matrix Size		68*68	68*68
Flip Angle		6°	6°
Number of Signal Averages		1	1
Triggering Frequency (min^{-1})		60	60
Cartesian	TE/TR (ms)	3.6/6.4	3.2/6.0
	Readout time (ms)	3.2	3.2
	Segmentation factor (pulsatile studies)	2	2
	Number of phases (pulsatile studies)	15	15
Spiral 12	TE/TR (ms)	2/13	1.57/13
	Readout time (ms)	9	9
	Segmentation factor (pulsatile studies)	1	1
	Number of phases (pulsatile studies)	15	15
Spiral 24	TE/TR (ms)	2/10	1.57/9.9
	Readout time (ms)	6	6
	Segmentation factor (pulsatile studies)	1	1
	Number of phases (pulsatile study)	15	15
Spiral 36	TE/TR (ms)	2/8.8	1.57/8.4
	Readout time (ms)	4	4
	Segmentation factor (pulsatile studies)	2	2
	Number of phases (pulsatile studies)	14	14

4D, four dimensional; TE, echo time; TR, repetition time; Venc, is the maximum allowed velocity corresponding to π phase shift.

[a] For pulsatile flows, segmented acquisition was used. Segmentation factor refers to number of acquired k-space line in each segment.

Table 2

Scan Time and RRMSE for Conventional 4D Flow and 4D Spiral Flow Acquisitions for Steady and Pulsatile Flow Rates at Distal Region to Stenosis.[a]

			Q = 50 ml/s	Q = 150 ml/s
Steady Flow	Cartesian	Scan time (min:s)	1:01	0:51
		RRMSE distal (%)	2.90	30.90
	Spiral 12	Scan time (min:s)	0:18	0:18
		RRMSE distal (%)	11.52	38.15
	Spiral 24	Scan time (min:s)	0:40	0:38
		RRMSE distal (%)	11.45	26.65
	Spiral 36	Scan time (min:s)	0:51	0:48
		RRMSE distal (%)	9.70	25.54
Pulsatile Flow	Cartesian	Scan time (min:s)	14:20	14:20
		RRMSE distal (%)	11.96	26.82
	Spiral 12	Scan time (min:s)	5:14	5:14
		RRMSE distal (%)	23.75	31.09
	Spiral 24	Scan time (min:s)	10:26	10:26
		RRMSE distal (%)	19.08	33.40
	Spiral 36	Scan time (min:s)	7:50	7:50
		RRMSE distal (%)	11.81	26.81

4D, four dimensional; RRMSE, relative root mean squared error.

[a]See Supporting Figure S5.

Table 3

Measured Parameters Using Conventional 4D Flow and 4D Spiral Flow in Five Normal Volunteers and Four Patients Suffering From Aortic Stenosis.[a]

Subject	MRI Modality	Peak Velocity (cm/s)	Time to Peak Velocity (ms)	AV Eject Time (ms)
N1	Conventional 4D	168	97	320
	4D spiral	180	97	320
N2	Conventional 4D	132	95	300
	4D spiral	161	93	310
N3	Conventional 4D	139	94	300
	4D spiral	139	93	320
N4	Conventional 4D	142	80	280
	4D spiral	168	77	300
N5	Conventional 4D	179	94	270
	4D spiral	184	93	280
P1	Conventional 4D	252	95	325
	4D spiral	266	95	330
	Doppler	278	140	325
P2	Conventional 4D	366	154	370
	4D spiral	385	154	370
	Doppler	391	125	340
P3	Conventional 4D	242	94	320
	4D spiral	240	94	310
	Doppler	217	100	320
P4	Conventional 4D	278	94	315
	4D spiral	277	93	335
	Doppler	293	95	280

AV, aortic valve; 4D, four dimensional.

[a]In the case of patients, we also report on corresponding Doppler-derived parameters. Peak velocity is peak systolic velocity measured during cardiac cycle. Time to peak is time from first image (slightly after onset of R-wave) to peak measureable systolic velocity. Eject time is effective systolic time measured.

Table 4

Results of Bland-Altman Analyses, Performed Between Each MR Modality and Doppler Ultrasound for Each of Three Indices Considered[a]

Measured Parameter	Two Modalities	Number of Subjects	Bias	Agreement Limits
Peak velocity	DUS and C4DF	4	10.25	(−36.83, 57.33)
	DUS and 4DSF	4	2.75	(−31.85, 37.35)
Time to peak	DUS and C4DF	4	−5.75	(−65.31, 53.81)
	DUS and 4DSF	4	−6	(−65.47, 53.47)
AV Eject time	DUS and C4DF	4	−16.25	(−53.24, 20.74)
	DUS and 4DSF	4	−20	(−76.01, 36.01)

AV, aortic valve; 4DSF = four-dimensional spiral flow, C4DF = conventional 4D flow; DUS = Doppler ultrasound.

[a]Peak velocity; time to peak; AV eject time.